

Experimental and computational studies on zwitterionic (E)-2-(1-(2-(4-methylphenylsulfonamido)ethyliminio)ethyl) phenolate

Gökhan Alpaslan · Hasan Tanak ·
Ayşen Alaman Ağar · Ahmet Erdönmez ·
Şamil Işık

Received: 16 April 2010/Accepted: 6 July 2010/Published online: 18 July 2010
© Springer Science+Business Media, LLC 2010

Abstract The Schiff base compound (E)-2-(1-(2-(4-methylphenylsulfonamido)ethyliminio)ethyl) phenolate has been synthesised and characterized by IR, UV–Vis, and X-ray single-crystal determination. Ab initio calculations have been carried out for the title compound using the density functional theory (DFT) and Hartree–Fock (HF) methods at 6-31G(d) basis set. The calculated results show that the DFT/B3LYP and HF can well reproduce the structure of the title compound. Using the TD-DFT and TD-HF methods, electronic absorption spectra of the title compound have been predicted and a good agreement with the TD-DFT method and the experimental ones is determined. Molecular orbital coefficient analyses reveal that the electronic transitions are mainly assigned to $n \rightarrow \pi^*$ and $\pi \rightarrow \pi^*$ electronic transitions. To investigate the tautomeric stability, optimization calculations at B3LYP/6-31G(d) level were performed for the NH and OH forms of the title compound. Calculated results reveal that the OH form is more stable than NH form. In addition, molecular electrostatic potential and NBO analysis of the title compound were performed at B3LYP/6-31G(d) level of theory.

Keywords Schiff base · Zwitterionic · MEP · NBO · DFT · HF

Introduction

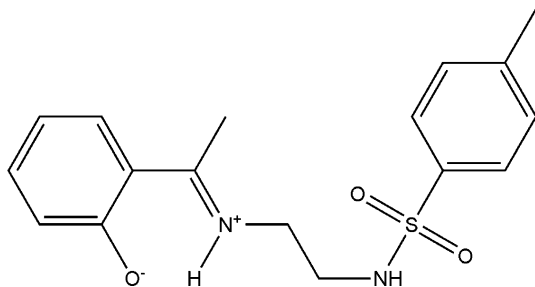
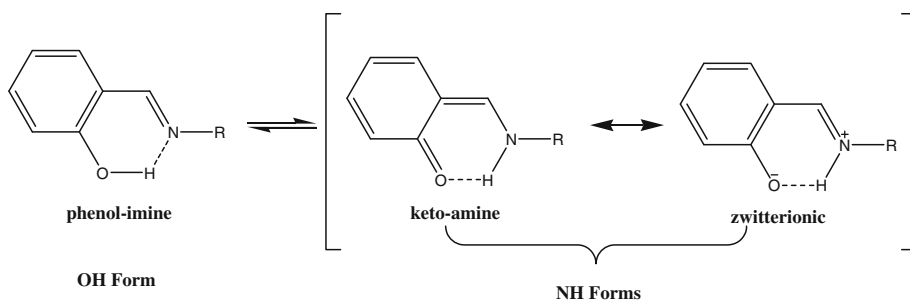
Schiff bases and their complexes are of great interest in many fields of chemistry and biochemistry because of their versatile metal-binding ability [1, 2]. Moreover, Schiff bases also have biological activities such as antimicrobial [3, 4], antifungal [5], antitumor [6, 7] activities, and herbicidal properties [8]. On the industrial scale, they have a wide range of applications, such as in dyes and in pigments [9]. Schiff base compounds display interesting photochromic and thermochromic features in the solid state and can be classified in terms of these properties [10]. Photo- and thermo-chromism arise via H-atom transfer from the hydroxy O atom to the N atom [11, 12]. Such proton exchanging materials can be utilized for the design of various molecular electronic devices [13]. In general, Schiff bases display two possible tautomeric forms, the phenol-imine (OH) and the keto-amine (NH) forms. Depending on the tautomers, two types of intramolecular hydrogen bonds are observed in Schiff bases: O–H···N in phenol-imine [14, 15] and N–H···O in keto-amine [16–18] tautomers (Scheme 1).

Although Schiff bases exhibit two possible tautomeric forms, OH and NH, another structural form, the zwitterion, is also observed. Zwitterionic forms of Schiff bases are regarded as a variant of their NH forms, but they can easily be distinguished from keto (NH) tautomers by their N⁺–H bond distances [19]. Zwitterionic forms of Schiff bases have an intramolecular ionic hydrogen bond (N⁺–H···O[−]), and their N⁺–H bonds are longer than the standard interatomic separations observed in neutral N–H bonds (0.87 Å) [19]. The other ionic bonds in the zwitterions, C=N⁺ and C–O[−], are not as distinctive as indicators as is the N⁺–H bond, because the NH form of Schiff bases in the solid state can be regarded as a resonance hybrid of two canonical

G. Alpaslan · H. Tanak (✉) · A. Erdönmez · Ş. Işık
Department of Physics, Faculty of Arts and Sciences,
Ondokuz Mayıs University, Kurupelit, 55139 Samsun, Turkey
e-mail: htanak@omu.edu.tr

A. A. Ağar
Department of Chemistry, Faculty of Arts and Sciences,
Ondokuz Mayıs University, Kurupelit, 55139 Samsun, Turkey

Scheme 1 Tautomeric forms of *o*-hydroxy Schiff bases



Scheme 2 (E)-2-(1-(2-(4-methylphenylsulfonamido)ethyliminio)ethyl)phenolate ($C_{17}H_{20}N_2O_3S$)

structures, namely the keto tautomer and the zwitterionic form [20, 21]. Different methods were used to show the presence of the enol, keto, and zwitterionic forms, among them are UV–Vis, IR, MS, 1H -, ^{13}C -, ^{14}N -NMR spectroscopy, and X-ray crystallography techniques [22–29].

In this article, we report the synthesis, characterization, and crystal structure of the Schiff base compound (E)-2-(1-(2-(4-methylphenylsulfonamido)ethyliminio)ethyl) phenolate (Scheme 2) as well as the theoretical studies on it using the HF/6-31G(d) and DFT/B3LYP/6-31G(d) methods. The properties of the structural geometry, molecular electrostatic potential (MEP), and natural bond orbital (NBO) analysis for the title compound at the B3LYP/6-31G(d) level were studied. These studies are valuable for providing insight into molecular properties of Schiff base compounds.

Experimental and computational methods

Synthesis

The compound (E)-2-(1-(2-(4-methylphenylsulfonamido)ethyliminio)ethyl) phenolate was prepared by reflux a mixture of a solution containing 2-hydroxyacetophenone (0.05 g 0.367 mmol) in 20-mL ethanol and a solution containing *N*-(2-aminoethyl)-*p*-toluenesulfonamide (0.078 g 0.367 mmol) in 20-mL ethanol. The reaction mixture was stirred for 1 h under reflux. The crystals of (E)-2-(1-(2-(4-methylphenylsulfonamido)ethyliminio)ethyl)phenolate

suitable for X-ray analysis were obtained from ethylalcohol by slow evaporation (Yield: % 54; m.p., 421–423 K). Chemical diagram of the title compound is shown in Scheme 2.

Crystal structure determination

A yellow crystal of the compound with dimensions of $0.50 \times 0.41 \times 0.32$ mm³ was mounted on goniometer of a STOE IPDS II diffractometer. Measurements were performed at room temperature (296 K) using graphite monochromated MoK α radiation ($\lambda = 0.71073$ Å). The systematic absences and intensity symmetries indicated the monoclinic $P2_1/n$ space group. A total of 9145 reflection (2705 unique) within the θ range of $[2.06^\circ < \theta < 26.0^\circ]$ were collected in the w scan mode. Cell parameters were determined using X-AREA software [30]. The intensities collected were corrected for Lorentz and polarization factors, absorption correction ($\mu = 0.21$ mm⁻¹) by integration method via X-RED32 software [30]. The structure was solved by direct methods using SHELXS-97 [31]. The maximum peaks and deepest hole observed in the final $\Delta\rho$ map were 0.24 and -0.27 eÅ⁻³, respectively. The scattering factors were taken from SHELXL-97 [31]. The molecular graphics were done using ORTEP-3 for Windows [32]. The data collection conditions and parameters of refinement process are listed in Table 1.

Computational methods

The molecular geometry is directly taken from the X-ray diffraction experimental result without any constraints. In the next step, the DFT calculations with a hybrid functional B3LYP (Becke's Three parameter hybrid functional using the LYP correlation functional) at 6-31G(d) basis set and the Hartree–Fock calculations at 6-31G(d) basis set by the Berny method [33, 34] were performed with the Gaussian 03W software package [35] and Gaussview visualization program [36]. The vibrational frequency calculations at the same levels of theory revealed no imaginary frequencies, indicating that an optimal geometry at these levels of approximation was found for the title

Table 1 Crystallographic data for the title compound

Crystal data	
Chemical formula	C ₁₇ H ₂₀ N ₂ O ₃ S
Crystal shape/color	Prism/yellow
Formula weight	332.41
Crystal system	Monoclinic
Space group	P2 ₁ /n
Unit cell parameters	$a = 11.4472(6)$ Å $b = 11.1176(4)$ Å $c = 13.4873(7)$ Å
Volume	1639.36(13) Å ³
Z	4
D_x (Mg cm ⁻³)	1.347
μ (mm ⁻¹)	0.214
F_{000}	704
Crystal size (mm ³)	0.50 × 0.41 × 0.32
Data collection	
Diffractometer/meas. meth	STOE IPDS II/w-scan
Absorption correction	Integration
T_{\min}	0.903
T_{\max}	0.954
No. of measured, independent and observed reflections	9145, 3194, 2705
Criterion for observed reflections	$I > 2\sigma(I)$
R_{int}	0.023
θ_{\max}	26
Refinement	
Refinement on	F^2
$R[F^2 > 2\sigma(F^2)]$, wR, S	0.034, 0.097, 1.05
No. of reflection	3194
No. of parameters	219
Weighting scheme	$w = 1/[\sigma^2(F_0^2) + (0.0843P)^2]$ $P = (F_0^2 + 2F_c^2)/3$
$(\Delta/\sigma)_{\max}$	0.001
$\Delta\rho_{\max}, \Delta\rho_{\min}$ (e Å ⁻³)	0.24, -0.27

compound. The electronic absorption spectra were calculated using the time-dependent density functional theory (TD-DFT) and Hartree–Fock (TD-HF) methods [37–40]. Also, it is calculated in ethanol solution using the Polarizable Continuum Model (PCM) [41–44]. To investigate the tautomeric stability, some properties such as total energy, HOMO and LUMO energies, and the chemical hardness [45] for the OH and NH forms of the title compound were obtained at B3LYP/6-31G(d) level in gas phase. These properties were also examined for the title compound in solvent media with three kinds of solvent (chloroform, ethanol, and water) using the PCM method.

To investigate the reactive sites of the title compound the molecular electrostatic potential was evaluated using

the B3LYP/6-31G(d) method. The molecular electrostatic potential, $V(r)$, at a given point $r(x, y, z)$ in the vicinity of a molecule, is defined in terms of the interaction energy between the electrical charge generated by the molecule's electrons and nuclei and a positive test charge (a proton) located at r . For the system studied the $V(r)$ values were calculated as described previously using the equation [46],

$$V(r) = \sum_A \frac{Z_A}{R_A - r} - \int \frac{\rho(r')}{r' - r} dr' \quad (1)$$

where Z_A is the charge of nucleus A, located at R_A , $\rho(r')$ is the electronic density function of the molecule, and r' is the dummy integration variable. In addition, NBO analysis was performed at the B3LYP/6-31G(d) level by means of the NBO 3.1 program within the Gaussian 03W package [47].

Results and discussion

Description of the crystal structure

The title compound, an Ortep-3 view of which is shown in Fig. 1, crystallizes in the monoclinic space group P2₁/n with $Z = 4$ in the unit cell. The asymmetric unit in the crystal structure contains only one molecule. The molecule adopts a folded conformation and dihedral angle between the aromatic ring systems is 6.57(5) $^\circ$. It is also known that Schiff bases may exhibit photochromism depending on the planarity or non-planarity, respectively [48]. The C7=N1 [1.303(2) Å] and C2–O1 [1.301(2) Å] bonds of the title compound are the most important indicators of the tautomeric type. While the C2–O1 bond is of a double bond for the keto-amine tautomer, this bond displays single bond character in phenol-imine tautomer. In addition, the C7–N1 bond is also a double bond in phenol-imine tautomer and of single bond length in keto-amine tautomer [49, 50]. However, these bond distances have intermediate values between single and double C–O (1.362 and 1.222 Å, respectively) and C–N (1.339 and 1.279 Å, respectively) bond distance [51]. The shortened C2–O1 bond and the slightly longer C7–N1 bond provide structural evidence for the zwitterionic tautomeric form of the title compound. Additionally, the bonds of C1–C7, C7–N1, and N1–C9 with their respective bond distances of 1.443(2), 1.303(2), and 1.457(2) Å indicate the zwitterionic character of the title compound [52]. The bond lengths of the title compound are in good agreement with those of the related structures 2-[*(E*)-2-(4-methylbenzenesulfonamido)ethyli-miniomethyl]-4-nitrophenolate [53] and (*E*)-2-hydroxy-6-[*(4*-propylphenyl)iminiomethyl]phenolate [54].

The title compound is stabilized by N–H···O and C–H···O type hydrogen bonds. There is a strong

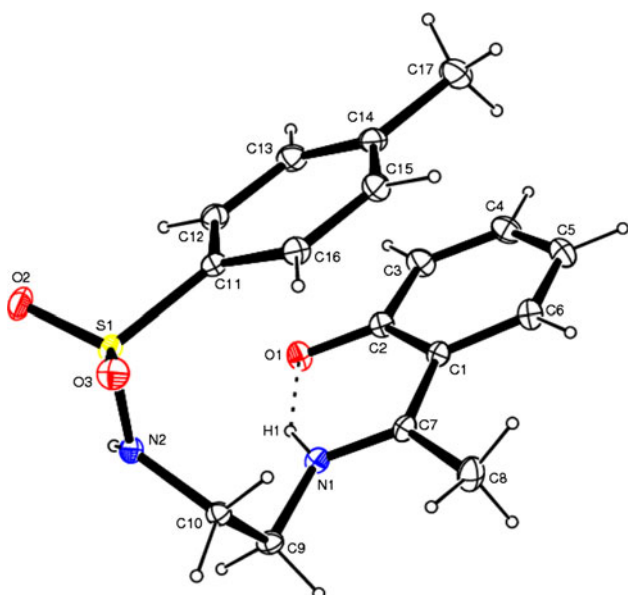


Fig. 1 Ortep 3 diagram of the title compound. Displacement ellipsoids are drawn at the 50% probability level and H atoms are shown as small spheres of arbitrary radii

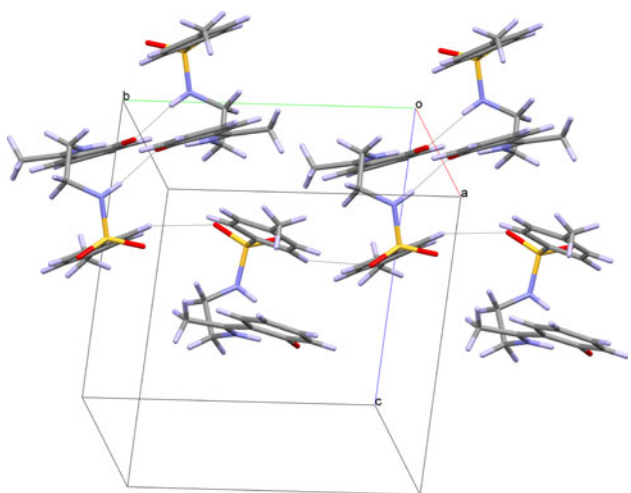


Fig. 2 Packing diagram of the title compound

Table 2 Hydrogen-bond geometry (\AA , $^\circ$)

D–H…A	D–H	H…A	D…A	D–H…A
N1–H1…O1	0.91(2)	1.68(2)	2.5056(17)	149(2)
N2–H18…O1 ⁱ	0.838(19)	1.949(19)	2.7816(17)	172.4(18)
C12–H12…O3 ⁱⁱ	0.93	2.51	3.309(2)	143.8
C17–H17C…Cg1 ⁱⁱⁱ	0.96	3.185	3.937 (3)	136

Note: Symmetry transformations used to generate equivalent atoms. (Cg1 is the centroid of the C1–C6 ring)

D donor, *A* acceptor

(i) $1 - x, -y, -z$; (ii) $3/2 - x, -1/2 + y, 1/2 - z$; (iii) $1/2 + x, 1/2 - y, 1/2 + z$

intramolecular $\text{N}1^+–\text{H}1…\text{O}1^-$ hydrogen bond (Fig. 1) with $\text{N}1…\text{O}1$ distance shorter than the sum of the van der Waals radii of O and N (3.07 Å) [55]. Atom N2 in the molecule at (x, y, z) act as hydrogen-bond donor to atom O1 in the molecule at $(1 - x, -y, -z)$, so forming a cyclic centrosymmetric $R_2^2(18)$ [56] dimer centered. The C–H…O hydrogen bonds link the molecules into a C(5) chain along the *b* axis (Fig. 2). In addition, there is a C–H…π interaction of C17–H17C and the phenyl ring. Perpendicular distance between atom H17C and the plane of the phenyl ring is 3.185 Å. The details of the hydrogen bonds are summarized in Table 2.

Optimized geometries

The optimized parameters (bond lengths, bond angles, and dihedral angles) of the title compound have been obtained at HF and B3LYP methods with the 6-31G(d) basis set. The calculated results are listed in Table 3. When the X-ray structure of the compound is compared with its optimized counterparts (see Fig. 3), conformational discrepancies are observed between them. The most remarkable discrepancies exist in the orientation of the phenyl and tolyl rings in the compound. According to X-ray study, dihedral angle between these two rings is 6.57(5) $^\circ$, whereas it has been calculated as 66.77 $^\circ$ for B3LYP and 64.04 $^\circ$ for HF. The orientation of the both the rings is defined by the torsion angles C2–C1–C7–N1 [$-5.3(2)^\circ$], C7–N1–C9–C10 [85.04(19) $^\circ$], C9–C10–N2–S1 [$-135.82(12)^\circ$] and N2–S1–C11–C16 [$-100.86(13)^\circ$] which have been calculated as 9.77 $^\circ$, 100.61 $^\circ$, 160.74 $^\circ$, and -95.12° for B3LYP, and 11.20 $^\circ$, 94.03 $^\circ$, 160.64 $^\circ$, and -98.12° for HF, respectively.

As seen from Table 3, most of the calculated bond lengths and the bond angles are slightly different from the experimental ones. We noted that the experimental results belong to the solid phase and theoretical calculations belong to the gaseous phase. In the solid state the experimental results are related to molecular packing, but in gas phase the isolated molecules are considered in the theoretical calculations. The biggest differences of bond lengths between the experimental and the predicted values are found at N2–S1 bond with the difference being 0.081 Å for B3LYP method, and C4–C5 bond with a value 0.059 Å for HF method. While the biggest differences for the bond angles are found as 3.96 $^\circ$ at C7–N1–C9 for B3LYP and 3.56 $^\circ$ at N1–C7–C8 for HF. According to above comparisons, the biggest differences of bond lengths and bond angles mainly occur in the groups involved in the hydrogen bonds [i.e., N2–S1, C4–C5, C7–N1–C9 and N1–C7–C8], which can also easily be understood taking into account the intra- and intermolecular hydrogen bond interactions present in the crystal.

Table 3 Selected molecular structure parameters

Parameters	Experimental	HF/ 6-31G(d)	B3LYP/ 6-31G(d)
Bond lengths (Å)			
C1–C6	1.410(2)	1.439	1.427
C1–C2	1.425(2)	1.462	1.467
C1–C7	1.443(2)	1.405	1.426
C2–O1	1.301(2)	1.235	1.278
C2–C3	1.416(2)	1.452	1.438
C3–C4	1.365(3)	1.344	1.371
C4–C5	1.374(3)	1.433	1.421
C5–C6	1.366(3)	1.345	1.372
C7–N1	1.303(2)	1.322	1.330
C7–C8	1.490(2)	1.509	1.508
C9–N1	1.457(2)	1.449	1.454
C9–C10	1.519(2)	1.527	1.538
C10–N2	1.4577(19)	1.455	1.463
C11–C16	1.382(2)	1.383	1.395
C11–C12	1.385(2)	1.390	1.398
C11–S1	1.7613(16)	1.771	1.797
C12–C13	1.373(3)	1.379	1.391
C13–C14	1.387(3)	1.394	1.403
C14–C15	1.378(3)	1.387	1.400
C14–C17	1.509(3)	1.510	1.510
C15–C16	1.378(3)	1.386	1.395
N2–S1	1.6011(13)	1.638	1.683
O2–S1	1.4245(12)	1.426	1.461
O3–S1	1.4313(12)	1.430	1.465
Max dif.		0.059	0.081
RMSE		0.0261	0.0283
Bond angles (°)			
C6–C1–C2	118.88(15)	118.38	119.10
C6–C1–C7	121.13(15)	121.81	121.10
C2–C1–C7	119.91(15)	119.77	119.64
O1–C2–C3	120.87(16)	119.74	120.29
O1–C2–C1	122.10(14)	123.81	123.13
C3–C2–C1	117.02(16)	116.42	116.57
C4–C3–C2	121.67(19)	121.86	121.81
C3–C4–C5	121.24(19)	121.60	121.28
C6–C5–C4	119.27(19)	119.18	119.36
C5–C6–C1	121.88(19)	122.48	121.83
N1–C7–C1	118.85(14)	120.17	117.88
N1–C7–C8	120.10(15)	116.54	120.20
C1–C7–C8	121.00(15)	123.27	121.90
N1–C9–C10	112.69(13)	111.41	110.05
N2–C10–C9	111.06(12)	109.71	110.08
C16–C11–C12	120.25(16)	120.44	120.77
C16–C11–S1	120.38(12)	120.12	119.86
C12–C11–S1	119.33(13)	119.43	119.34
C13–C12–C11	119.20(17)	119.44	119.19
C12–C13–C14	121.60(17)	121.04	121.22

Table 3 continued

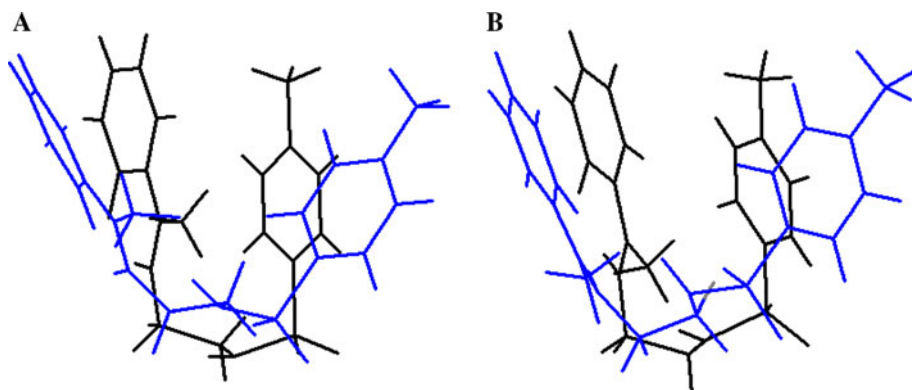
Parameters	Experimental	HF/ 6-31G(d)	B3LYP/ 6-31G(d)
C15–C14–C13	118.13(17)	118.58	118.39
C15–C14–C17	120.88(19)	121.22	121.05
C13–C14–C17	120.99(19)	120.18	120.53
C14–C15–C16	121.43(17)	121.00	121.19
C15–C16–C11	119.38(16)	119.47	119.21
C7–N1–C9	126.26(14)	128.93	130.22
C10–N2–S1	119.36(11)	120.52	118.96
O2–S1–O3	119.13(8)	121.88	122.64
O2–S1–N2	106.72(8)	105.78	105.56
O3–S1–N2	107.86(7)	106.55	106.11
O2–S1–C11	108.17(8)	107.58	107.45
O3–S1–C11	107.16(8)	107.34	107.42
N2–S1–C11	107.28(7)	106.84	106.69
Max dif.		3.56	3.96
RMSE		1.227	1.181
Torsion angles (°)			
C10–C9–N1–C7	85.04(19)	94.03	100.61
C9–C10–N2–S1	-135.82(12)	160.64	160.74
C12–C11–S1–N2	77.15(14)	81.37	83.80
C10–N2–S1–C11	65.17(12)	70.46	71.10
N1–C9–C10–N2	69.28(17)	60.10	59.26
C2–C1–C7–N1	-5.3(2)	11.20	9.77
C6–C1–C7–N1	177.99(15)	-170.90	-174.58

In order to compare the theoretical results with the experimental values, root mean square error (RMSE) is used and the values of which for bond lengths and bond angles are calculated as 0.0283 Å and 1.181° for B3LYP method, and 0.0261 Å and 1.227° for HF method. A logical method for globally comparing the structures obtained with the theoretical calculations is by superimposing the molecular skeleton with that obtained from X-ray diffraction, giving a RMSE of 1.792 Å for B3LYP and 1.837 Å for method HF (Fig. 3). According to these results, it may be concluded that while the HF calculations well reproduce the bond lengths, the B3LYP method is better in predicting the bond angles and 3-D geometry of the title compound.

IR spectroscopy

The FT-IR spectra of the title compound were recorded in the 4000–400 cm⁻¹ region using KBr pellets on a Schmadzu FT-IR 8900 spectrophotometer. The spectra contain some characteristic bands of the stretching vibrations of the NH, CH, CN, CO, and SO₂ groups. The IR spectrum of the title compound shows two bands at 3371

Fig. 3 Atom-by-atom superimposition of the structures calculated (**a** = HF; **b** = DFT) over the X-ray structure for the title compound



and 3191 cm^{-1} due to N–H stretching vibrations. This difference between the N–H stretching vibration frequencies is because of the intramolecular $\text{N}1^+ \cdots \text{H}1 \cdots \text{O}1^-$ hydrogen bonding which leads a shift to lower wavenumber. The weak bands in the range $3070\text{--}3000\text{ cm}^{-1}$ correspond to the symmetric and asymmetric stretching vibrations of aromatic and methyl CH bonds. The characteristic region of $1500\text{--}1700\text{ cm}^{-1}$ can be used to identify the proton transfer of Schiff bases. The title compound shows a strong band at 1610 cm^{-1} which is assigned to C=N stretching vibration. Another characteristic region of the Schiff bases derivative spectrum is $1100\text{--}1400\text{ cm}^{-1}$, which is attributed to C–O stretching vibrations. The C–O stretching vibration was observed at 1388 cm^{-1} which confirms the presence of phenolate group in the compound. The symmetric and asymmetric SO_2 stretching vibrations can occur in the regions $1125\text{--}1150$ and $1295\text{--}1330\text{ cm}^{-1}$, respectively [57]. In our study, these SO_2 stretching vibrations were observed at 1064 and 1285 cm^{-1} . The presence of N–H, C=N, and C–O stretching vibrations strongly suggest that the title compound has the zwitterionic form in the solid state.

Electronic absorption spectra

The UV–Vis electronic absorption spectra of the title compound were recorded within 200–600-nm range on a Unicam UV–Vis spectrophotometer in EtOH solvent. The observed spectra showed three bands at 360 ($\log \epsilon = 5.008$), 288 ($\log \epsilon = 4.657$), and 242 nm ($\log \epsilon = 4.628$). The maximum absorption wavelength is assigned to intramolecular electronic transfer band of the C=N group which contributes to $n \rightarrow \pi^*$ transition and the other bands may be due to $\pi \rightarrow \pi^*$ transitions of the phenyl and tolyl rings. These values are similar to those found in related compound [29]. According to some studies on the UV–Vis spectrum of *o*-hydroxylated Schiff bases, the band at $>400\text{ nm}$ indicates presence of the keto-amine form [58–61]. In our study, any band belonging to keto-amine form was not observed with a value greater than 400 nm ,

which indicates that the title compound is in zwitterionic form and not in keto in ethanol solvent.

Electronic absorption spectra of the title compound were calculated by TD-DFT and TD-HF methods based on the B3LYP/6-31G(d) and HF/6-31G(d) levels optimized structure in gas phase, respectively. For TD-HF calculations, the absorption wavelengths are obtained at 297 , 215 , and 176 nm . It is obvious that these bands are not corresponding to the experimental results, which shows that using the TD-HF method here to predict the electronic absorption spectra is not reasonable. For TD-DFT calculations, the theoretical absorption bands are predicted at 388 , 275 , and 224 nm and can easily be seen that they correspond to the experimental absorption ones. In addition to the calculations in gas phase, TD-DFT calculations of the title compound in ethanol solvent were performed by using PCM model. The PCM calculations reveal that the calculated absorption bands have slight blue-shifts with values of 379 , 269 , and 221 nm when compared with the

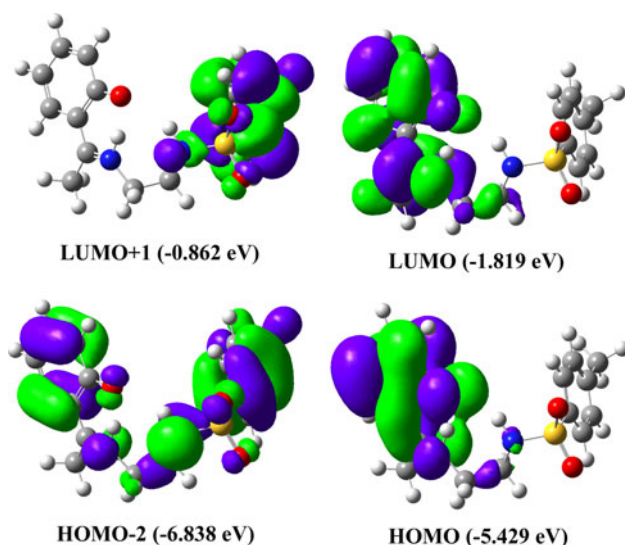


Fig. 4 Molecular orbital surfaces and energy levels given in parentheses for the HOMO – 2, HOMO, LUMO, and LUMO + 1 of the title compound computed at B3LYP/6-31G(d) level

gas-phase calculations of TD-DFT method. According to the investigation on the frontier molecular orbital (FMO) energy levels of the title compound, we can find that the corresponding electronic transfers happened between the highest occupied molecular orbital (HOMO) and the lowest unoccupied molecular orbital (LUMO), HOMO – 2 and LUMO, HOMO – 2 and LUMO + 1 orbitals, respectively. Figure 4 shows the distributions and energy levels of the FMOs computed at the B3LYP/6-31G(d) level for the title compound. As seen from Fig. 4, in the HOMO and LUMO, electrons are mainly delocalized on the phenolate ring and the atoms of imine group; in the LUMO + 1, electrons are delocalized on the tolyl ring and sulfonamide fragment and in the HOMO – 2, electrons are delocalized on the whole structure.

Molecular orbital coefficients analyses based on optimized geometry indicate that, for the title compound, the frontier molecular orbitals are mainly composed of *p*-atomic orbitals, so aforementioned electronic transitions are mainly derived from the contribution of bands $n \rightarrow \pi^*$ and $\pi \rightarrow \pi^*$.

Energetics and stability

The NH and OH tautomerism of the title compound is given in Scheme 1. To investigate the tautomeric stability, optimization calculations at B3LYP/6-31G(d) level were performed for the NH and OH forms of the title compound. Some physicochemical properties such as total, HOMO, and LUMO energies, dipole moment and chemical hardness (η) were also calculated with the same level of theory and the results were given in Table 4. The chemical hardness is quite useful to rationalize the relative stability and reactivity of chemical species. Hard species having large HOMO–LUMO gap will be more stable and less reactive than soft species having small HOMO–LUMO gap [62]. As seen from Table 4, the total energy of the OH form is lower than the NH form, while chemical hardness of the OH form is greater than the NH one, which indicates that the OH form of the title compound is more stable than its NH form in gas phase.

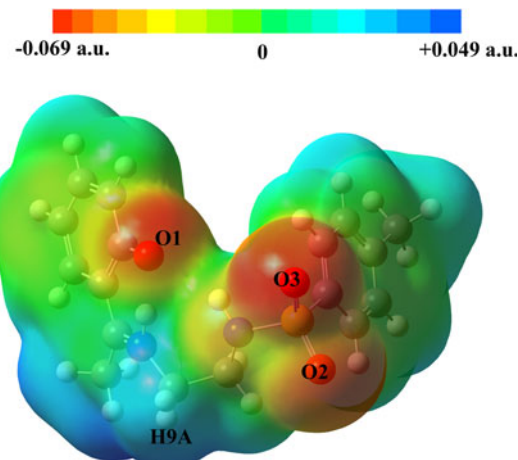


Fig. 5 Molecular electrostatic potential map calculated at B3LYP/6-31G(d) level

In order to evaluate the solvent effect to the aforementioned properties of the title compound, we carried out calculations in three kinds of solvent (water, ethanol, and chloroform) with the B3LYP/6-31G(d) level using the PCM model and the results are given in Table 4. From Table 4, we can conclude that the total molecular energies obtained by PCM method decrease with the increasing polarity of the solvent, while the dipole moments and hardness will increase with the increase of the polarity of the solvent. According to these results, the stability of the title compound increases in going from the gas phase to the solution phase.

Molecular electrostatic potential

MEP is related to the electronic density and is a very useful descriptor in determining sites for electrophilic and nucleophilic reactions as well as hydrogen bonding interactions [63, 64]. The electrostatic potential $V(r)$ is also well suited for analyzing processes based on the “recognition” of one molecule by another, as in drug–receptor and enzyme–substrate interactions, because it is through their potentials that the two species first “see” each other [65, 66].

Table 4 Calculated energies, dipole moments, frontier orbital energies, and harnesses

	OH form gas phase ($\varepsilon = 1$)	NH form gas phase ($\varepsilon = 1$)	Chloroform ($\varepsilon = 4.9$)	Ethanol ($\varepsilon = 24.55$)	Water ($\varepsilon = 78.39$)
E_{total} (Hartree)	−1393.153562	−1393.150209	−1393.163211	−1393.167035	−1393.167751
E_{HOMO} (eV)	−5.959	−5.429	−5.396	−5.387	−5.386
E_{LUMO} (eV)	−1.439	−1.819	−1.712	−1.681	−1.675
η (eV)	2.26	1.805	1.842	1.853	1.855
μ (D)	8.102	8.385	9.696	10.139	10.225

Table 5 Second-order perturbation theory analysis of the Fock matrix in NBO basis, calculated at B3LYP/6-31G(d) level

Donor orbital (<i>i</i>)	Acceptor orbital (<i>j</i>)	$E^{(2)c}$ (kcal/mol)	$\epsilon_j - \epsilon_i$ (a.u.) ^a	F_{ij} (a.u.) ^b
LP(1) O1	BD(1) N1–H1	6.28	1.40	0.084
LP(2) O1	BD(1) N1–H1	17.76	0.97	0.119
LP(1) O1	BD(1) N2–H18	5.14	1.62	0.082
LP(2) O1	BD(1) N2–H18	2.85	1.19	0.053
LP(3) O1	BD(1) N2–H18	1.50	1.17	0.041
LP(1) O3	BD(1) C12–H12	0.61	1.56	0.027
LP(3) O3	BD(1) C12–H12	0.49	1.09	0.022

^a Energy difference between donor and acceptor *i* and *j* NBO orbitals

^b F_{ij} is the Fock matrix element between *i* and *j* NBO orbitals

^c $E^{(2)}$ means energy of hyper conjugative interactions

To predict reactive sites for electrophilic or nucleophilic attack for the investigated molecule, the MEP at the B3LYP/6-31G(d) optimized geometry was calculated. The negative (red) regions of the MEP are related to electrophilic reactivity and positive (blue) regions to nucleophilic reactivity, as shown in Fig. 5. As can be seen from the figure, this molecule has several possible sites for electrophilic attack. Negative electrostatic potential regions (red color) are mainly localized over the O1 atom and the O2 and O3 atoms of the sulfonamide group. The negative $V(r)$ values are -0.069 a.u. for O3 atom which is the most negative region, -0.067 a.u. for O1 atom and -0.064 a.u. for O2 atom. However, a maximum positive region (blue color) is localized on the C9–H9A bond with a value of $+0.049$ a.u., indicating a possible site for nucleophilic attack. According to these calculated results, the MEP map shows that the negative potential sites are on oxygen atoms as well as the positive potential sites are around the hydrogen atoms. These sites give information concerning the region from where the compound can have metallic bondings and intermolecular interactions. So, Fig. 5 confirms the existence of the intermolecular C12–H12···O3 and N2–H18···O1 interactions.

NBO analysis

NBO analysis provides an efficient method for studying intra- and intermolecular bonding and interaction among bonds, and also provides a convenient basis for investigating charge transfer or conjugative interaction in molecular systems [67]. The larger the $E^{(2)}$ value, the more intensive is the interaction between electron donors and electron acceptors, i.e., the more donating tendency from electron donors to electron acceptors and the greater the extent of conjugation of the whole system. Delocalization of electron density between occupied Lewis-type (bond or lone pair) NBO orbitals and

formally unoccupied (antibond or Rydberg) non-Lewis NBO orbitals correspond to a stabilizing donor–acceptor interaction.

In order to investigate the intra and intermolecular interactions, the stabilization energies of the title compound were performed by using second-order perturbation theory. For each donor NBO(*i*) and acceptor NBO(*j*), the stabilization energy $E^{(2)}$ associated with electron delocalization between donor and acceptor is estimated as [68, 69]

$$E^{(2)} = -q_i \frac{(F_{ij})^2}{\epsilon_j - \epsilon_i} \quad (2)$$

where q_i is the donor orbital occupancy, ϵ_j , ϵ_i are diagonal elements (orbital energies), and F_{ij} is the off-diagonal NBO Fock matrix element. The results of second-order perturbation theory analysis of the Fock Matrix at B3LYP/6-31G(d) level of theory are presented in Table 5.

NBO analysis revealed that the $n(\text{O1}) \rightarrow \sigma(\text{N1–H1})$ interactions give the strongest stabilization to the system of the title compound by 24.04 kcal mol $^{-1}$, and strengthen the intramolecular N1–H1···O1 hydrogen bond. The lone pairs of O1 also donate its electrons to σ -type antibonding orbital for N2–H18. The total stabilization energy of N2–H18···O1 intermolecular hydrogen bonding is 9.49 kcal mol $^{-1}$. There is another NBO interaction of the $n(\text{O3}) \rightarrow \sigma(\text{C12–H12})$ imply the existence of C12–H12···O3 hydrogen bond which has the total stabilization energy 1.1 kcal mol $^{-1}$. We can say that the energy of the C12–H12···O3 hydrogen bond we obtained is reliable when it is compared with some values in literature. For example, Desiraju [70] has estimated the energy of the C–H···O hydrogen bond as 1.0 – 2.0 kcal mol $^{-1}$.

Thus, it is apparent that N–H···O and C–H···O intermolecular interactions significantly influence crystal packing in this molecule.

Conclusions

(E)-2-(1-(4-Methylphenylsulfonamido)ethyliminio)ethyl phenolate has been synthesized and characterized by IR, UV–Vis, and X-ray single-crystal diffraction. The X-ray, IR, and UV–Vis spectral data for the title compound show that the compound exists in the zwitterionic form, which is stabilized by the intramolecular $\text{N}^+ \cdots \text{H} \cdots \text{O}^-$ hydrogen bond. The HF and DFT calculations show that the predicted geometries can reproduce the structural parameters; however, the intermolecular interactions have some influences on the molecular geometry in the solid state. The TD-DFT calculations lead to a very closer agreement with the experimental absorption spectra both gas phase and solvent media. Molecular orbital coefficient analyses suggest that the electronic transitions are mainly assigned to $n \rightarrow \pi^*$ and $\pi \rightarrow \pi^*$ electronic transitions. The MEP map shows that the negative potential sites are on oxygen atoms as well as the positive potential sites are around the hydrogen atoms. These sites give information about the region from where the compound can have intermolecular interactions and metallic bonding. NBO analysis revealed that the $n(\text{O}1) \rightarrow \sigma(\text{N}1-\text{H}1)$ interaction gives the strongest stabilization to the system, and the major interaction for the intermolecular $\text{O}1 \cdots \text{N}2$ contact is $n(\text{O}1) \rightarrow \sigma(\text{N}2-\text{H}18)$.

Supplementary data

CCDC-691752 contains the supplementary crystallographic data for the compound reported in this paper. These data can be obtained free of charge at www.ccdc.cam.ac.uk/conts/retrieving.html [or from the Cambridge Crystallographic Data Centre (CCDC), 12 Union Road, Cambridge CB2 1EZ, UK; fax: +44(0)1223-336033; e-mail: deposit@ccdc.cam.ac.uk].

References

- Calligaris M, Randaccio L (1987) In: Wilkinson G (ed) Comprehensive coordination chemistry, vol 2. Pergamon, London, pp 715–738
- Zhou Y-S, Zhang L-J, Zeng X-R, Vital JJ, You X-Z (2000) J Mol Struct 553:25–30
- El-Masry AH, Fahmy HH, Abdelwahed SHA (2000) Molecules 5:1429–1438
- Pandey SN, Sriram D, Nath G, De Clercq E (1999) II Farmaco 54:624–628
- Singh WM, Dash BC (1988) Pesticides 22:33–37
- Hodnett EM, Dunn WJ (1970) J Med Chem 13:768–770
- Desai SB, Desai PB, Desai KR (2001) Heterocycl Commun 7:83–90
- Holla BS, Rao BS, Shridhara K, Akberali PM (2000) II Farmaco 55:338–344
- Taggi AE, Hafez AM, Wack H, Young B, Ferraris D, Lectka T (2002) J Am Chem Soc 124:6626–6635
- Cohen MD, Schmidt GMJ, Flavian S (1964) J Chem Soc 2041–2051
- Hadjoudis E, Vitterakis M, Mavridis IM (1987) Tetrahedron 43:1345–1360
- Xu X-X, You X-Z, Sun Z-F, Wang X, Liu H-X (1994) Acta Crystallogr C50:1169–1171
- Alarcon SH, Pagani D, Bacigalupo J, Olivieri AC (1999) J Mol Struct 475:233–240
- Petek H, Albayrak Ç, Ağar E, Ocak İskeli N, Şenel I (2007) Acta Cryst E63:o810–o812
- Özek A, Albayrak Ç, Odabaşoğlu M, Büyükgüngör O (2007) Acta Cryst C63:o177–o180
- Karabiyik H, Ocak İskeli N, Petek H, Albayrak Ç, Ağar E (2008) J Mol Struct 873:130–136
- Koşar B, Büyükgüngör O, Albayrak Ç, Odabaşoğlu M (2004) Acta Cryst C60:o458–o460
- Tanak H, Erşahin F, Koysal Y, Ağar E, Işık Ş, Yavuz M (2009) J Mol Mod 15:1281–1290
- Petek H, Albayrak Ç, Odabaşoğlu M, Şenel I, Büyükgüngör O (2010) Struct Chem. doi: [10.1007/s11224-010-9598-6](https://doi.org/10.1007/s11224-010-9598-6)
- Ogawa K, Harada J (2003) J Mol Struct 647:211
- Karabiyik H, Guzel B, Aygün M, Boğa G, Büyükgüngör O (2007) Acta Cryst C63:o215
- Ünver H (2001) Spectrosc Lett 34:783
- Salman SR, Lindon JC, Farrant RD (1991) Spectrosc Lett 24: 1071
- Salman SR, Lindon JC, Farrant RD (1993) Magn Reson Chem 31:991
- Alarcon SH, Olivieri AC, Nordon A (1995) Tetrahedron 51:4619
- Bingöl Alpaslan Y, Tanak H, Ağar E, Erşahin F (2009) Acta Cryst E65:1842
- Tanak H, Yavuz M (2010) J Mol Mod 16:577–587
- Bingöl Alpaslan Y, Alpaslan G, Ağar A, Işık Ş (2010) Acta Cryst E66:o510
- Trzesowska-Kruszynska A (2010) Struct Chem. doi: [10.1007/s11224-009-9547-4](https://doi.org/10.1007/s11224-009-9547-4)
- Cie Stoe (2002) X-AREA (Version 1.18) and X-RED32 (Version 1.04). Stoe & Cie, Darmstadt
- Sheldrick GM (1997) SHELXS97 and SHELXL97. University of Göttingen, Göttingen
- Burnett MN, Johnson CK (1996) ORTEP 3 Report ORNL-6895. Oak Ridge National Laboratory, Oak Ridge
- Schlegel HB (1982) J Comput Chem 3:163
- Peng C, Ayala PY, Schlegel HB, Frisch MJ (1996) J Comput Chem 17:49
- Frisch MJ, Trucks GW, Schlegel HB, Scuseria GE, Robb MA, Cheeseman JR, Montgomery JA Jr, Vreven T, Kudin KN, Burant JC, Millam JM, Iyengar SS, Tomasi J, Barone V, Mennucci B, Cossi M, Scalmani G, Rega N, Petersson GA, Nakatsuji H, Hada M, Ehara M, Toyota K, Fukuda R, Hasegawa J, Ishida M, Nakajima T, Honda Y, Kitao O, Nakai H, Klene M, Li X, Knox JE, Hratchian HP, Cross JB, Bakken V, Adamo C, Jaramillo J, Gomperts R, Stratmann RE, Yazyev O, Austin AJ, Cammi R, Pomelli C, Ochterski JW, Ayala PY, Morokuma K, Voth GA, Salvador P, Dannenberg JJ, Zakrzewski VG, Dapprich S, Daniels AD, Strain MC, Farkas O, Malick DK, Rabuck AD, Raghavachari K, Foresman JB, Ortiz JV, Cui Q, Baboul AG, Clifford S, Cioslowski J, Stefanov BB, Liu G, Liashenko A, Piskorz P, Komaromi I, Martin RL, Fox DJ, Keith T, Al-Laham MA, Peng CY, Nanayakkara A, Challacombe M, Gill PMW, Johnson B, Chen W, Wong MW, Gonzalez C, Pople JA (2004) Gaussian 03, Revision E.01. Gaussian Inc, Wallingford

36. Frisch A, Dennington R II, Keith T, Millam J, Nielsen AB, Holder AJ, Hiscock J (2007) GaussView Reference, Version 4.0. Gaussian Inc, Pittsburgh
37. Runge E, Gross EKU (1984) Phys Rev Lett 52:997–1000
38. Stratmann RE, Scuseria GE, Frisch MJ (1998) J Chem Phys 109:8218–8224
39. Bauernschmitt R, Ahlrichs R (1996) Chem Phys Lett 256: 454–464
40. Casida ME, Jamorski C, Casida KC, Salahub DR (1998) J Chem Phys 108:4439–4449
41. Miertus S, Scrocco E, Tomasi J (1981) Chem Phys 55:117–129
42. Barone V, Cossi M (1998) J Phys Chem A 102:1995–2001
43. Cossi M, Rega N, Scalmani G, Barone V (2003) J Comput Chem 24:669–681
44. Tomasi J, Mennucci B, Cammi R (2005) Chem Rev 105: 2999–3094
45. Parr RG, Pearson RG (1983) J Am Chem Soc 105:7512
46. Politzer P, Murray J (2002) Theor Chem Acc 108:134–142
47. Glendening ED, Badenhoop JK, Reed AE, Carpenter JE, Weinhold F (1995) NBO Version 3.1. Theoretical Chemistry Institute, University of Wisconsin, Madison
48. Moustakali-Mavridis I, Hadjoudis E, Mavridis A (1978) Acta Cryst B34:3709–3715
49. Petek H, Albayrak Ç, Odabaşoğlu M, Şenel I, Büyükgüngör O (2008) J Chem Crystallogr 38:901–905
50. Albayrak Ç, Koşar B, Demir S, Odabaşoğlu M, Büyükgüngör O (2010) J Mol Struct 963:211–218
51. Allen FH, Kennard O, Watson DG, Brammer L, Orpen AG, Taylor R (1987) J Chem Soc Perkin Trans 2:S1–S19
52. Petek H, Albayrak Ç, Ocak-İskeleli N, Ağar E, Şenel I (2007) J Chem Crystallogr 37:285–290
53. Tüfekçi M, Alpaslan G, Macit M, Erdönmez A (2009) Acta Cryst E65:o2143
54. Yazıcı S, Albayrak Ç, Gümrükçüoglu I, Şenel I, Büyükgüngör O (2010) Acta Cryst E66:o93
55. Bondi A (1964) J Phys Chem 68:441–450
56. Bernstein J, Davies RE, Shimoni L, Chang NL (1995) Angew Chem Int Ed Engl 34:1555
57. Bellamy LJ (1980) The infrared spectra of complex molecules. Chapman and Hall, London vol. 2
58. Yıldız M, Kılıç Z, Hökelek T (1998) J Mol Struct 441:1–10
59. Nazır H, Yıldız M, Yılmaz H, Tahir MN, Ülkü D (2000) J Mol Struct 524:241–250
60. Ünver H, Yıldız M, Zengin DM, Özbeş S, Kendi E (2001) J Chem Crystallogr 31:211–216
61. Salman SR, Kamounah FS (2002) Spectrosc Lett 35:327–335
62. Özbek N, Kavak G, Özcan Y, İde S, Karacan N (2009) J Mol Struct 919:154–159
63. Scrocco E, Tomasi J (1978) Adv Quantum Chem 11:115–121
64. Luque FJ, Lopez JM, Orozco M (2000) Theor Chem Acc 103: 343–345
65. Politzer P, Laurence PR, Jayasuriya K, McKinney J (1985) Environ Health Perspect 61:191–202
66. Scrocco E, Tomasi J (1973) Topics in current chemistry, vol 7. Springer, Berlin, p 95
67. Snehalatha M, Ravikumar C, Hubert Joe I, Sekar N, Jayakumar VS (2009) Spectrochim Acta A 72:654–662
68. Schwenke DW, Truhlar DG (1985) J Chem Phys 82:2418
69. Gutowski M, Chalasinski G (1993) J Chem Phys 98:4728
70. Desiraju GR (1991) Acc Chem Res 24:290–296